Hindawi
Journal of Chemistry
Volume 2023, Article ID 2162991, 12 pages
https://doi.org/10.1155/2023/2162991

Research Article

A DFT and TD-DFT Study of Two Hydralazine Derivatives for Organic Solar Cells and Nonlinear Optical Applications

Remi Nkeih Tamighang,[1] Dodo Lydie Ajifack,[1] Stanley Numbonui Tasheh,[1] Nyiang Kennet Nkungli,[1] Charly Tedjeuguim Tsapi,[2] and Julius Numbonui Ghogomu[1,2]

[1]*Department of Chemistry, Faculty of Science, The University of Bamenda, P. O Box 39, Bambili, Bamenda, Cameroon*
[2]*Department of Chemistry, Research Unit of Noxious Chemistry and Environmental Engineering, Faculty of Science, University of Dschang, P.O. Box 67, Dschang, Cameroon*

Correspondence should be addressed to Julius Numbonui Ghogomu; ghogsjuju@hotmail.com

Received 25 April 2023; Revised 2 June 2023; Accepted 25 November 2023; Published 8 December 2023

Academic Editor: J. O. Caceres

In recent years, organic molecules have been the subject of in-depth research studies using *in silico* methods for their applications in solar cells and photonic devices. This study reports a theoretical investigation of the organic solar cell (OSC) and nonlinear optical (NLO) properties of (E)-1-(phthalazin-1-yl)-1-[(pyridin-2-yl)ethylidene]hydralazine (**PPEH**) and 1-[2-(1-(pyridine-3- yl) ethylidene)hydrazinyl]phthalazine (**PEHP**). The density functional theory (DFT) and its time-dependent extension (TD-DFT) were employed with the B2PLYP, M06-2X, BP86, CAM-B3LYP, and ω B97-XD functionals, alongside the def2-tzvp and def2-tzvpp basis sets. Geometrical and Frontier molecular orbital (FMO) analyses were performed. Reactivity descriptors, open circuit voltage (V_{oc}), energy driving force (ΔE_{L-L}), light harvesting efficiencies (LHEs), NLO susceptibilities, and properties were also computed and discussed. The results show that **PEPH** and **PPEH** are good electron donor materials for organic solar cells as they possess high FMO energies, V_{ocs}, ΔE_{L-Ls}, and LHEs. Moreover, both molecules have static first and second hyperpolarizabilities as well as dynamic NLO responses that are on average 10 times greater than those of *para*-nitroaniline. **PEPH** and **PPEH** also exhibit properties such as second harmonic generation (SHG), electro-optic Pockels effect (EOPE), electric field-induced second harmonic generation (EFISHG), and optical Kerr effect (OKE). Indeed, these molecules are potential candidates for organic solar cells and NLO applications. Findings from this work may further accelerate the synthesis and development of green energy materials for optical solar cells and NLO applications in the future.

1. Introduction

Organic photovoltaic devices such as organic solar cells (OSCs) and organic light-emitting diodes (OLEDs) are state-of-the-art technologies around the world, with research in these areas steadily increasing [1–6]. This is a result of their environmental friendliness, ease of assembly, low cost and physical flexibility [7]. Despite significant advancements in the search for better optoelectronic components, finding high-performance, tiny, and thermally stable organic-based photovoltaic systems are still challenging. This points out how crucial it is to create new organic materials with a variety of functionalities for better optoelectronic device performance. Among the aforementioned photovoltaic devices, OSCs can directly convert sunlight into electrical energy [8, 9]. It constitutes an organic film sandwiched between two electrodes [1, 6, 10]. The materials used to create this film are both donors and acceptors, mounted in a two-layer structural configuration. The fullerene (6,6)-phenyl-C61-butyric acid methyl ester (PCBM) is commonly used as an electron acceptor material in OSCs [11–13], whereas poly(3-hexylthiophene) (P3HT) and its derivatives are widely employed as electron donor materials in OSC devices [11, 14]. Accordingly, P3HT and PCBM were used herein as reference materials for the design of OSCs.

The design of photovoltaic systems have equally benefited from nonlinear optical (NLO) features brought about by a material's particles oscillating in response to an external applied electric field [15]. Effective NLO molecules are known to be π-conjugated systems and possess electron acceptor (A) and donor (D) groups [16–20]. These molecules are known as push-pull or D-π-A molecules. The NLO activities of these push-pull molecules are caused by intramolecular charge transfer between D and A [20]. Alterations of the structural as well as functional groups, typically by adding more powerful electron donor/acceptor groups and/or changing the type and length of the spacer, are frequently used to enhance the NLO responses of materials [14]. It is worth mentioning that optical switches and sensors, modulators, optical computing, optical data processing, optical data storage, optical limiting effects, and holography are just a few applications of NLO materials [20–22].

Due to the superior characteristics of organic materials, such as their ultrafast response times, lower dielectric constants, high internal quantum efficiency, high damage threshold, and flexible design [23], more organic materials than their inorganic counterparts have been the subject of electronic quality research in recent years [14, 24–26].

Hydralazine hydrazone-based organic compounds such as (E)-1-(phthalazin-1-yl)-1-[(pyridin-2-yl)ethylidene]hydralazine (**PPEH**) and 1-[2-(1-(pyridine-3- yl)ethylidene) hydrazinyl]phthalazine (**PEHP**), synthesized, partially characterized, and screened for their antiplasmodial, antimicrobial, and antioxidant activities by Awantu and collaborators [27] (see Figure 1) are among the organic materials which are likely to have high charge transport capabilities. The structural features of these molecules are donor-π-acceptor-π-donor (D-π-A-π-D) like, which is most likely to enhance intramolecular charge transfer where the donor (D) plays the role of hole transport and the acceptor (A) functions as an electron transporter [14, 17]. Moreover, their extended π-skeleton is a precondition for significant NLO activities. The synthesis, crystal structure, antifungal, and antionchocercal activities of similar compounds have also been reported [28–30].

Despite the fascinating structural characteristics of **PEHP** and **PPEH** that are amendable to organic solar cell and nonlinear optical applications, there is no comprehensive study of the OSC and NLO properties of these molecules in the literature. Thus, research into these perspectives is necessary. This work sought to theoretically provide insights into the design of **PEHP** and **PPEH** as potential materials for applications in optical solar cell and NLO devices, through the prediction of OSC and NLO parameters. To achieve this, geometrical analysis was performed, open circuit voltage (V_{oc}), the energy driving force (ΔE_{L-L}), electronic adsorption spectra, linear, and nonlinear parameters were computed and discussed. The density functional theory (DFT) and its time-dependent extension (TD-DFT) were chosen for this study because they reflect a reliable alternative for addressing these tasks, as the methodology investigates electronic structure and spectroscopic properties of these types of materials [31]. Again, the theoretical approach is the best tool for overcoming experimental synthesis difficulties and exploring substitutes that reduce material production and processing costs. DFT was also chosen due to its ability to account for electron correlation at a lower computational cost and the balance between computation time and accuracy [16, 21]. The findings from this study will provide insights about the electronic and optical properties of two hydralazine derivatives, contributing to the development of organic solar cells and nonlinear optical applications.

2. Computational Details

Apart from the NLO-related computations, all quantum chemical calculations in this work were done with the ORCA 4.0.1 quantum chemical package [32]. NLO activities were predicted with the Gaussian 16 program package [33]. In all ORCA calculations, the medium-sized numerical quadrature grid 5 and the tight self-consistent field (SCF) convergence criterion were used. Input structures were prepared using the Avogadro 1.1.1 program [34]. Geometry optimization and frequency calculations were performed using the BP86 Generalized Gradient Approximation (GGA) functional [35] and the def2-TZVP Ahlrichs basis set [36, 37]. The resolution-of-the-identity (RI-J) approximation [38] in combination with the chain-of-spheres (COSX) approximation, giving rise to the RIJ-COSX approximation, was utilised to speed up the geometry optimization and frequency calculations with negligible accuracy sacrifice. Analysis of vibrational frequencies shows no imaginary frequency, establishing that all optimized geometries were stable structures (minima on the potential energy surface).

Based on the BP86-optimized geometries, single-point (SP) calculations were performed using the double hybrid-GGA functional B2PLYP (with 53% Hartree–Fock and 27% second-order møller plesset perturbation (MP2) [39, 40] and M06-2X (with 54% Hartree–Fock (HF)) [41] along with the Karlsruhe basis set def2-tzvpp [42]. The M06-2X and B2PLYP functionals were employed here due to their effectiveness in energy calculations and their ability to model noncovalent interactions [40, 41]. Long-range dispersion interactions within the studied molecules were accounted for through Grimme's atom pair-wise dispersion correction with Becke–Johnson's damping dubbed (D3BJ) [43], except for the M06-2X functional, where the D3zero [41] dispersion correction was used. Absorption spectra and NLO properties of the investigated compounds were computed at CAM-B3LYP/def2-tzvpp and ω B97-XD/def2-tzvpp levels of theory.

Based on the fact that HOMO and LUMO energy levels of materials are the main determinants of their OSCs quality, some major Frontier molecular orbital (FMO) energy level-based parameters were computed in this study. These include the energy driving force (ΔE_{L-L}), which is the difference between the LUMO energy levels of the donor (the hydralazines studied) and the acceptor (PCBM, a reference material), as well as the open circuit voltage (V_{OC}) which was calculated according to the following equation:

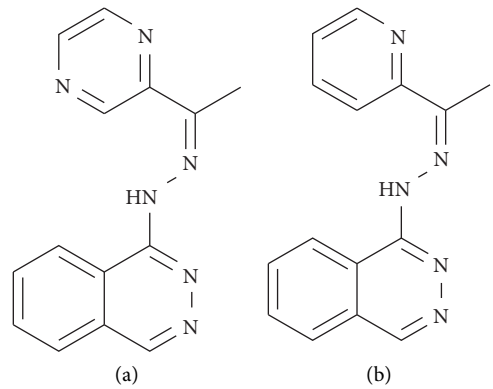

Figure 1: Chemical structures of (a) (E)-1-(phthalazin-1-yl)-1-[(pyridin-2-yl)ethylidene]hydralazine (PPEH) and (b) 1-[2-(1-(pyridine-3-yl)ethylidene)hydrazinyl]phthalazine (PEHP).

$$V_{oc} = \left(\left[E_{HOMO}^{donor}\right] - \left[E_{LUMO}^{acceptor}\right]\right) - 0.3, \quad (1)$$

where 0.3 is an empirical factor, E_{HOMO}^{donor} is the HOMO energy of the donor molecule, $E_{LUMO}^{acceptor}$ is the LUMO energy of the acceptor material, and V_{oc} is the open circuit voltage.

The dissociation efficiency at the donor/acceptor interface in OSC devices is determined by the energy difference (ΔE_{L-L}) in LUMO energies of donor and acceptor molecules, which were calculated as shown in the following equation:

$$\Delta E_{L-L} = \text{LUMO}^{\text{donor}} - \text{LUMO}^{aceptor}. \quad (2)$$

Within this framework, dissociation is only possible when the values of ΔE_{L-L} are less than 0.3 eV [5, 44].

Light harvesting efficiency (LHE) refers to a material's ability to produce excitons after photon absorption. Thus, it can serve as an important metric in understanding the efficiency optical solar cells [45]. It is worth noting here that, the charge transfer process in solar cells is primarily influenced by LHE values [46]. The LHEs for this study were calculated using the oscillator strengths obtained by TD-DFT calculation according to the following equation:

$$\text{LHE} = 1 - 10^{-f}, \quad (3)$$

where f is the oscillator strength of the molecule associated to the maximum absorption wavelength.

Components of the static and dynamic electronic linear polarizability (α), the quadratic hyperpolarizability (β), and the cubic hyperpolarizability (γ) tensors were calculated to determine the linear and nonlinear optical properties of **PEPH** and **PPEH**. The static dipole polarizabilities [α (0; 0)], first hyperpolarizabilities [β (0; 0, 0)], and second hyperpolarizabilities [γ (0; 0, 0, 0)] were calculated at frequency $\omega = 0$. On the other hand, the dynamic polarizabilities [α ($-\omega$; ω)], first hyperpolarizabilities [(-2ω; ω, ω)], the vector components of the first hyperpolarizabilities projected along the dipole moment [β_{vec}], and the electric field-induced second harmonic generation (EFISHG) [γ (-2ω; ω, ω, 0)] were calculated at $\omega = 0.04282$ a.u.

The induced microscopic polarizability (P), which occurs when a molecule is exposed to an oscillating external electric field produced by strong light, like laser light, can be expressed as a power series in the electric field E as shown in the following equation [47–49]:

$$p = \sum_{j} \alpha_{ij} E_j + \sum_{j \le k} \beta_{ijk} E_j E_k + \sum_{j \ge K \ge l} \gamma_{ijk} E_j E_k E_l + \cdots, \quad (4)$$

where α, β, and γ are the linear polarizability, first (quadratic) hyperpolarizability, and second (cubic) hyperpolarizability tensors, respectively.

In this study, equations (5) and (6) were employed to calculate the average linear polarizability $\langle\alpha\rangle$ and the total static first hyperpolarizability (β_{tot}). Equations (7) and (8) in turn, were used to compute the vector part of the dynamic first hyperpolarizability (β_{vec}), and the average (isotropic) second hyperpolarizability (γ), respectively.

$$\langle\alpha\rangle = \frac{1}{3}\left(\alpha_{xx} + \alpha_{yy} + \alpha_{zz}\right), \quad (5)$$

$$\beta_{tot} = \left(\beta_x^2 + \beta_y^2 + \beta_z^2\right)^{(1/2)}, \quad (6)$$

$$\beta_{vec} = \left(\beta_x^2 + \beta_y^2 + \beta_z^2\right)^{(1/2)}, \quad (7)$$

where $\beta_x = (\beta_{xxx} + \beta_{yyy} + \beta_{zzz})$, $\beta_y = (\beta_{yyy} + \beta_{yzz} + \beta_{yxx})$, $\beta_z = (\beta_{zzz} + \beta_{xxx} + \beta_{zyy})$.

$$\gamma = \frac{1}{5}\left[\gamma_{xxxx} + \gamma_{yyyy} + \gamma_{zzzz} + 2\left(\gamma_{xxyy} + \gamma_{xxzz} + \gamma_{yyzz}\right)\right]. \quad (8)$$

The isotropic values of the second harmonic generation (SHG) [β (-2ω; ω, ω)], electro-optic Pockels effect (EOPE) [β ($-\omega$; ω, 0)], electric field induced second harmonic generation (EFISHG) [γ (-2ω; ω, ω, 0)], and optical Kerr effect (OKE) [γ (0; ω, $-\omega$, 0)] were as well calculated in addition to the aforementioned hyperpolarizabilities. These hyperpolarizabilities are relevant to this study because they can frequently be obtained from experiments and frequently serve as a reference for comparing data obtained from various sources [50].

3. Results and Discussion

3.1. Structural Analysis. Presented in Figure 2 are the optimized structures of **PEPH** and **PPEH**. The optimized Cartesian coordinates of the studied compounds are provided in Tables S1 and S2 of the accompanying electronic supplementary material (ESM).

Table 1 displays the selected geometric parameters of the optimized structures.

Geometric parameters obtained theoretically at the BP86-D3(BJ)/def2-TZVP level are found to be consistent with experimental counterparts obtained from the CCDC 1007670 (crystallographic data). The optimized structures are therefore suitable for further analysis. Also presented in Table 1 are some dihedral angles of the studied molecules. Although the dihedral angles deviate slightly from the ideal 0° and 180° values in a perfect square planar geometry, the molecules remain significantly planar. Given that planarity in a molecule is caused by π-conjugation, intramolecular charge transfer between the electron donor and acceptor groups in the studied hydralazine derivatives is likely and may result in a significant OSC.

Linear regression between theoretical and experimental bond lengths was performed to further assess the suitability of the level of theory used and the optimized structures obtained as shown graphically in Figure S1 of the ESM. The regression curves yielded the following equations:

$$\begin{aligned} \text{Cal.} &= 0.9328\,\text{Exp.} + 0.073,\\ R^2 &= 0.9014 \ (\text{for } \mathbf{PEPH}),\\ \text{Cal.} &= 0.9484\,\text{Exp.} + 0.0526,\\ R^2 &= 0.9032 \ (\text{for } \mathbf{PPEH}). \end{aligned} \tag{9}$$

High correlation coefficients (R^2) are obtained between theoretical and experimental values in a good linear regression, demonstrating the suitability of the applied theory level and the optimized structures.

3.2. Chemical Stability of the Studied Molecules. Stability is a key quality of ideal materials for photovoltaic cells. Chemical stability is commonly defined by absolute chemical hardness (η), which measures the system's resistance to exchanging electron density with the surrounding environment [51]. η was computed as shown in the following equation:

$$\eta = \frac{1}{2}(\text{IP} - \text{EA}), \tag{10}$$

where IP is the ionisation potential and EA is the electron affinity of the system. The values of IP and EA were calculated using equations (11) and (12), respectively, at the B2PLYP-D3(BJ)/def2-tzvpp and M06-2X(D3Zero)/def2-tzvpp levels of theory in the gaseous phase, and the results are provided in Table 2. Listed in Table S3 of the ESM are the energies of the cationic (E^+), anionic (E^-), and neutral (E^0) species of the studied molecules in eV. The M06-2X and B2PLYP functionals were chosen here due to their outstanding performance in energy calculation [40, 41].

$$\text{IP} = E^+ - E^0, \tag{11}$$

$$\text{EA} = E^0 - E^-. \tag{12}$$

In these equations, E^+, E^-, and E^0 are single-point energies of the cationic, anionic, and neutral forms of the molecules investigated.

Results from Table 2 indicate that at both levels of theory, a similar trend is observed. The findings also depict that **PPEH** has a smaller η value (i.e., 3.872 eV for M06-2x and 3.473 eV for B2PLYP) when contrasted with **PEPH** (i.e., 3.964 eV for M06-2x and 3.562 eV for B2PLYP). This indicates that **PPEH** is relatively less stable and chemically more reactive than **PEPH**. Consequently, **PPEH** is expected to exhibit a higher charge transport rate as required in solar cells. All computed EA values are less than that of experimental oxygen molecule (0.448 eV) [52]. This signifies that the investigated compounds are less stable toward corrosion in the environment [53]. Accordingly, anticorrosive measures are recommended should these molecules be used as organic solar cell materials.

The M06-2X-D3(BJ)/def2-tzvpp level of theory is considered for subsequent discussions thanks to its effectiveness in modelling noncovalent interactions and electronic properties of organic molecules [41].

3.3. Photovoltaic Properties

3.3.1. Frontier Molecular Orbital (FMO) Analysis. The ability of charge to be transferred between the donor and acceptor components of a material is determined by their Frontier molecular orbital (FMO) energy levels [14, 54]. For an efficient charge transfer process, the HOMO and LUMO energies of the materials must be higher than the reference acceptor material, PCBM (HOMO = −6.10 eV and LUMO = −3.75 eV) and lower than that of P3HT (HOMO = −4.65 eV and LUMO = −2.13 eV), a reference donor molecule [14, 24]. To evaluate the ability of the studied molecules to act as charge transfer agents in solar cells, their HOMO and LUMO energies were calculated at M06-2X/def2-tzvpp level of theory in the gaseous phase as presented in Table 3.

The findings from the table indicate that the computed HOMO and LUMO energies of the studied molecules are lower than those of P3HT, but greater than those of PCBM. This indicates efficient injection of electrons into the lowest-lying unoccupied molecular orbital of the acceptor material. Resultantly, the studied molecules may serve as electron donor agents in organic solar cells. Moreover, this ability of photo-excited electron transfer from the investigated molecules to PCBM is of significant importance to both organic solar cells and most photovoltaic devices.

Also presented in Table 3 are the energy gap (E_{gap}) values of the compounds under investigation. The E_{gap} value of **PPEH** is slightly lower than that of **PEPH**. This indicates that **PPEH** is more reactive and less stable than **PEPH**. Consequently, **PPEH** is expected to be a better electron donor material in organic solar cells. The FMO iso-surfaces of the molecules studied as visualised with Avogadro 1.1.1 [34] are displayed in Figure 3.

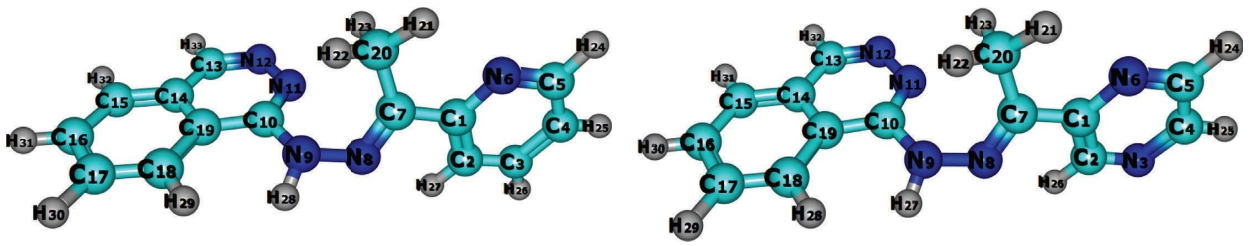

(a) (b)

Figure 2: Optimized structures of (a) PEPH and (b) PPEH as obtained at the BP86-D3(BJ)/def2-tzvp level of theory.

Table 1: Comparison of theoretical and experimental geometric parameters of PEPH and PPEH.

Geometric parameters	PEPH		PPEH	
	Cal	Exp	Cal	Exp
Bond lengths (Å)				
C1-C7	1.488	1.453	1.483	1.453
C7-C20	1.491	1.493	1.491	1.493
C7-N8	1.298	1.307	1.299	1.307
N8-N9	1.389	1.358	1.384	1.358
N9-C10	1.391	1.340	1.393	1.340
Bond angles (°)				
N6-C1-C7	116.7	114.6	117.7	114.6
C2-C1-C7	121.1	124.5	121.6	124.5
N8-C7-C1	114.9	112.2	114.5	112.2
N8-C7-C20	126.3	124.0	126.6	124.0
C7-N8-N9	117.8	122.4	118.1	122.4
N9-C10-C12	117.8	120.4	117.7	120.4
N9-C10-N11	118.5	120.0	118.5	120.0
Dihedral angles (°)				
N11-C10-N9-N8	8.7	—	7.3	—
C10-N9-N8-C7	64.1	—	62.1	—
N9-N8-C7-C20	4.9	—	5.4	—
N8-C7-C20-C1	177.2	—	176.9	—
C20-C7-C1-N6	11.0	—	11.5	—
N8-C7-C1-C2	14.1	—	15.3	—

Exp, experimental values; Cal, calculated values.

Table 2: Calculated chemical hardness (η), ionisation potential (IP), and electron affinity (EA) of the studied compounds in the gaseous phase.

Level of theory	Molecule	IP (eV)	EA (eV)	η
B2PLYP-D3(BJ)/def2-tzvpp	PEPH	7.314	0.190	3.562
	PPEH	7.334	0.387	3.473
M06-2X(D3zero)/def2-tzvpp	PEPH	7.433	0.307	3.964
	PPEH	7.622	0.312	3.872

Table 3: HOMO, LUMO energy, and E_{gap} values (all in eV) of the different molecules calculated at the M06-2X/def2-tzvpp level of theory in the gaseous phase.

Species	E_{HOMO}	E_{LUMO}	E_{gap}
P3HT	−4.65	−2.13	2.52
PEPH	−5.11	−2.64	2.47
PPEH	−5.25	−2.80	2.45
PCBM	−6.10	−3.75	2.35

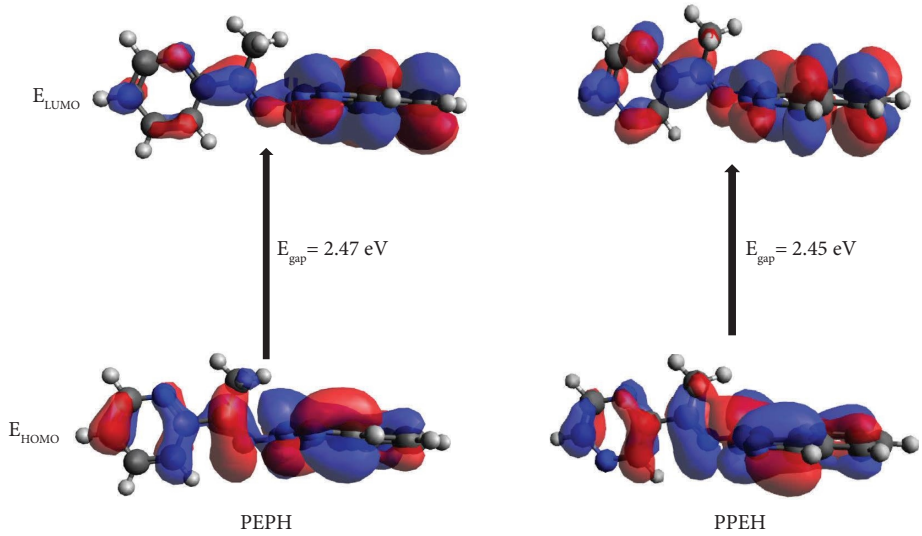

Figure 3: Frontier molecular orbitals of PEPH and PPEH obtained at the M06-2X/def2-tzvpp level of theory in the gaseous phase.

3.3.2. Open Circuit Voltage (V_{oc}). The open circuit voltage (V_{oc}) is an important factor that determines the efficiency of an organic solar cell. As initially defined V_{oc} is a function of the HOMO energy of the donor material and LUMO energy of the acceptor material, from which the rate of charge transfer is effectively determined [55, 56]. The computed V_{ocs} at the M06-2X/def2-tzvpp level of theory and those of the reference donor (P3HT) and acceptor materials (PCBM), along with the ΔE_{L-L} values are listed in Table 4.

The outcomes indicate that all the calculated values are greater than those of the prototypical materials: P3HT and PCBM. This demonstrates the ability of the molecules under study to introduce electrons into the open orbitals of the acceptor material PCBM. All of the investigated molecules can therefore be used as donor materials in organic solar cells. It is also clear from the table that the differences between the LUMO energy of the studied molecules and the LUMO of the reference acceptor material are far greater than 0.3 eV. This raises the possibility of a significant transfer of photo-excited electrons from the molecules under study to the acceptor material (PCBM), further confirming the ability of these molecules to be used in the fabrication of photovoltaic devices. The ΔE_{L-L} trend of the studied compounds varies as follows: **PPEH** < **PPEH**. Notably, this finding concurs with the chemical stability, E_{gap}, and FMO analysis, indicating the likelihood that **PPEH** will function well as charge transporters in photovoltaic devices.

3.4. Nonlinear Optical (NLO) Properties and Susceptibilities. Presented in Tables S4–S9 of the ESM are the tensor components of the nonlinear properties and susceptibilities used for this study.

3.4.1. Average Static Linear Polarizability Isotropies $\langle\alpha\rangle$. To predict the linear optical activities of the investigated compounds, their average linear polarizability isotropy $\langle\alpha\rangle$, which determines charge distribution and plays a key role in the intramolecular charge transfer (ICT) rate for linear optical response in materials, was computed [48, 49]. Here, the origin of Cartesian coordinate system $(x, y, z) = (0, 0, 0)$ was used as the centre of mass in each molecule. Presented in Table 5 are the average linear polarizability isotropies $\langle\alpha\rangle$ and its x, y, and z components computed at CAM-B3LYP/def2-tzvpp and wB97-XD/def2-tzvpp levels of theory. The range-separated functionals CAM-B3LYP and ωB97-XD were used here owing to their effectiveness to model the orbital energy of π-conjugated molecules that involve charge transfer in excited states [57, 58]. Also presented in this table are the values of *para*-nitroaniline, a prototypical push-pull chromophore for nonlinear optics, which was used as a reference. The following conversion factors were used in this work: 1 a.u. = 1.4819×10^{-24} esu for linear polarizability, 1 a.u. = 8.639418×10^{-33} esu for first hyperpolarizability and 1 a.u. = 5.0367×10^{-39} esu for second hyperpolarizability.

Table 4: Voc/PCBM and E_{L-L} (all in eV) of the different molecules calculated at the DFT/M06-2X/def2-tzvpp level of theory in the gas phase.

Species	E_{HOMO}	E_{LUMO}	V_{oc}/PCBM	ΔE_{L-L}
P3HT	−4.65	−2.13	0.60	1.62
PEPH	−5.11	−2.64	1.06	1.11
PPEH	−5.25	−2.80	1.20	0.95
PCBM	−6.10	−3.75	2.05	—

The results show that the $\langle\alpha\rangle$ values for the compounds examined at both levels are all higher (i.e., by about 2×10^{-22} esu times) and very similar to those of PNA for each level used. On this basis, **PEPH** and **PPEH** possess higher linear optical properties than PNA. The results also show that $\langle\alpha\rangle$ is dominant in the x-direction (see values for α_{xx} component in the table) for all compounds under investigation, suggesting that ICT occurs primarily in the x-direction, along which lies a bulk of the π-conjugated system of the molecules. In addition, **PEPH** has the highest $\langle\alpha\rangle$ values, which results in significant ICT required for linear optical applications.

Table 5: The average linear static polarizability $\langle\alpha\rangle \times 10^{-22}$ isotropies (in esu) and their x, y, and z components (in a.u.) of PEPH, PPEH, and PNA.

Compounds	Level of theory	α_{xx}	α_{yy}	α_{zz}	$\langle\alpha\rangle \times 10^{-22}$
PEPH	CAM-B3LYP/def2-tzvpp	348.32	181.93	143.36	3.327
	wB97-XD/def2-tzvpp	348.61	182.47	143.95	3.334
PPEH	CAM-B3LYP/def2-tzvpp	346.03	178.78	136.21	3.265
	wB97-XD/def2-tzvpp	346.28	179.26	136.88	3.272
PNA	CAM-B3LYP/def2-tzvpp	146.13	98.79	48.83	1.451
	wB97-XD/def2-tzvpp	145.59	98.95	49.17	1.451

3.4.2. Static First and Second Hyperpolarizabilities. To determine the susceptibilities of the investigated molecules to NLO activities in response to an applied static electric field, their static first (β_{tot}) and second hyperpolarizabilities $\langle\gamma\rangle$ were computed at $\omega = 0$. The static first and second hyperpolarizabilities are denoted β (0; 0, 0) and γ (0; 0, 0, 0), respectively. Tables 6 and 7 present the computed values of β (0; 0, 0) and γ (0; 0, 0, 0), respectively, at different levels of theory alongside their molecular tensor components along the x, y, and z cartesian coordinate axes.

The datasets depict that the computed values of β (0; 0, 0) and γ (0; 0, 0, 0) of the studied molecules are approximately 3.5 times greater than those of PNA at all levels of theory under investigation, indicating their likelihood of significant NLO activities. Consequently, they are promising NLO chromophores for use in optoelectronic devices. **PPEH** exhibits the largest β (0; 0, 0) and γ (0; 0, 0, 0) values at all study levels and is predicted to demonstrate more significant NLO activities.

3.4.3. Dynamic First Hyperpolarizability (β_{vec}). To determine the capability of the studied hydralazine molecules undergoing NLO activities in response to an applied dynamic (frequency dependent) electric field, the vector components of the dynamic first hyperpolarizability (β_{vec}) were calculated at the Nd: YAG laser wavelength (λ) of 1064 nm (i.e., at frequency, $\omega = 0.04282$ a.u.) and the results are listed in Table 8.

Table 8 demonstrates that the computed values of β_{vec} are significantly higher than those of PNA, demonstrating their potential for quadratic dynamic NLO effects at the specified light wavelength. It isIt's interesting to note that all computed values of β_{vec} at wavelength 1064 nm are positive and, as a result, parallel to the dipole moment vector. It is also obvious that **PPEH** has the largest computed values of β_{vec} across all levels of theory. This suggests that **PPEH** may exhibit a relatively more significant dynamic second-order NLO activity necessary for the design of optoelectronics and photonics devices. It is worth mentioning that the β_{vec} results are in line with those suggested by chemical stability, open circuit voltage v_{oc}, β_{tot}, β (0; 0, 0) and γ (0; 0, 0, 0). **PPEH** and **PEPH** are therefore promising materials for OSC and NLO devices.

3.4.4. NLO Properties (SHG, EOPE, EFISHG, and OKE). The NLO response of the investigated molecules was predicted through the second harmonic generation (SHG) [β (-2ω; ω, ω)], electro-optic Pockels effect (EOPE) [β ($-\omega$; ω, 0)], electric field-induced second harmonic generation (EFISHG) [γ (-2ω; ω, ω, 0)], and optical Kerr effect (OKE) [γ (0; ω, $-\omega$, 0)]. These results are listed in Table 9. The calculations were all carried out at the popular laser frequency of 0.08242 a.u. using the range-separated functionals CAM-B3LYP and ωB97-XD in conjunction with the def2-tzvpp Ahlrich basis set.

The findings indicate that the range-separated functionals CAM-B3LYP and ω B97-XD yield similar results, although those obtained with CAM-B3LYP are slightly higher. It can be inferred from Table 9 that the computed values of the dynamic first hyperpolarizabilities: SHG [β (-2ω; ω, ω)] and EOPE [β ($-\omega$; ω, 0)] of the studied molecules are greater than those of **PNA**. This suggests that they are potential candidates for Second Harmonic Generation and Electro-Optic Pockel's effect applications. The results also show that **PPEH** has the highest SHG and EOPE values at both levels of theory, and is expected to have significant SHG and EOPE activities, which are necessary for optoelectronic applications.

Moreover, the predicted values of EFISHG and OKE of the investigated molecules are higher than those of PNA, suggesting their applicability in optoelectronic and photonic devices. As expected, the calculated EFISHG and OKE values of **PPEH** are relatively larger than those of **PEPH** at both levels of theory. This confirms **PPEH** as a better NLO chromophore.

3.5. TD-DFT Study. The absorption wavelength (λ_{max}) of a suitable NLO material must satisfy certain absorption property requirements; otherwise, the undesirable optical transparency effect may occur. Due to strong electromagnetic (EM) absorption in the visible region (400–800 nm), optical transparency significantly reduces the properties of a material. Strong visible-range light absorption can result in high optical transparencies, limiting the NLO applications of materials [59, 60]. Moreover, materials which show intense absorption of light (characterized by high oscillator strength) are likely to undergo electronic transitions with charge transfer character that can enhance their nonlinear response [59, 60].

Table 6: Static total first hyperpolarizabilities (β_{tot}) and the x, y, and z components (in a.u.) for the investigated compounds, calculated at $\omega = 0$.

Compounds	Functional	β_x	β_y	β_z	β_{tot} x 10^{-30} esu
PEPH	CAM-B3LYP/def2-tzvpp	164.431	−306.450	−4.275	3.00
	wB97-XD/def2-tzvpp	181.233	−306.176	−4.572	3.07
PPEH	CAM-B3LYP/def2-tzvpp	−203.933	−344.709	−83.809	3.54
	wB97-XD/def2-tzvpp	−162.403	−342.327	−85.686	3.36
PNA	CAM-B3LYP/def2-tzvpp	282.566	0.005	−32.048	2.46
	wB97-XD/def2-tzvpp	237.198	0.004	−29.937	2.07

Table 7: Average static second hyperpolarizabilities $\langle\gamma\rangle$ in esu and its tensor components (in a.u.) of the studied compounds, calculated at $\omega = 0$.

Compounds	Level of theory	γ_{xxxx}	γ_{yyyy}	γ_{zzzz}	γ_{xxyy}	γ_{xxzz}	γ_{yyzz}	$\langle\gamma\rangle$x10^{-35}esu
PEPH	CAM-B3LYP/def2-tzvpp	363657	10596	7921	15570	5172	2527	4.32
	wB97-XD/def2-tzvpp	347646	10932	8333	15395	5219	2662	4.16
PPEH	CAM-B3LYP/def2-tzvpp	377550	10430	6790	15498	5169	2363	4.44
	wB97-XD/def2-tzvpp	361004	10813	7139	15368	5296	2491	4.28
PNA	CAM-B3LYP/def2-tzvpp	84173	5472	1888	−2095	305	832	0.90
	wB97-XD/def2-tzvpp	81800	5703	1951	−1893	332	879	0.89

Table 8: Dynamic first hyperpolarizbility, (β_{vec} in 10^{-30} esu) alongside its components (in a.u.) for PEPH, PPEH, and p-NA, calculated at $\lambda = 1064$ nm ($\omega = 0.04282$ a.u.).

Molecule	Level of theory	β_x	β_y	β_z	β_{vec}x 10^{-30}esu
PEPH	CAM-B3LYP/def2-tzvpp	196.375	−345.519	−4.985	3.43
	wB97-XD/def2-tzvpp	213.408	−344.516	−5.503	3.50
PPEH	CAM-B3LYP/def2-tzvpp	−253.801	−385.087	−96.919	4.07
	wB97-XD/def2-tzvpp	−206.459	−382.986	−93.824	3.85
PNA	CAM-B3LYP/def2-tzvpp	285.562	0.007	−34.921	2.47
	wB97-XD/def2-tzvpp	220.053	0.005	−32.249	1.90

Table 9: Frequency-dependent NLO properties (in 10^{-3} a.u.) of PEPH, PPEH, and PNA calculated at $\omega = 0.04282$ a.u.

NLO property	CAM-B3LYP/Def2-TZVPP			ωb97-XD/Def2-TZVPP		
	PEPH	PPEH	PNA	PEPH	PPEH	PNA
SHG [β (−2ω; ω, ω)]	0.55	0.67	0.21	0.56	0.62	0.20
EOPE [β (−ω; ω, 0)]	0.40	0.47	0.15	0.41	0.45	0.14
EFISHG[γ(−2ω; ω, ω, 0)]	51.85	54.88	10.08	48.95	51.67	9.85
OKE [γ(0; ω, −ω, 0)]	33.92	35.16	6.98	32.53	33.69	6.98

The UV-Vis absorption spectra of the investigated molecules were calculated using the TD-DFT method to ascertain whether the transparency-efficiency trade-off mentioned above might apply to them. The predicted absorption wavelength (λ_{abs}), excitation energy (E_{abs}), oscillator strength, orbital coefficients, dominant electronic transitions, and light harvesting efficiencies (LHEs) are listed in Table 10. The parameters in this table correspond to the absorption bands with the highest oscillator strengths, which represent the most intense band in the UV-Vis spectrum.

The findings reveal that both levels of theory employed here yield similar trends. However, discussion is based on that obtained by the CAM-B3LYP/def2-tzvpp level. The outcomes also show that **PEPH** and **PPEH** have oscillator strengths of 0.3617 and 0.3923, respectively. Interestingly, the computed values of λ_{max} at the specified levels of theory fall within the UV region of the EM spectrum (100–400 nm), indicating that the molecules strongly absorb in this region. The molecules are therefore likely to experience only minor optical losses, leading to a favourable nonlinear efficiency-accuracy trade-off. The electronic absorption energies are 3.971 and 3.941 eV for **PEPH** and **PPEH**, respectively. It can also be seen from Table 10 that the highest electronic absorption is due to the HOMO ⟶ LUMO electronic transition involving the S_0 and S_1 states.

The computed LHEs for PEPH and PPEH are 0.5652 and 0.5947, respectively, as shown in Table 10. As a result, the values of LHE are similar; hence, the studied molecules are

Table 10: Absorption wavelength, highest oscillator strength, main transitions (in %), and light harvesting efficiencies of PEPH and PPEH computed at CAM-B3LYP/def2-tzvpp and ω B97-XD/def2-tzvpp levels of theory.

Level of theory	Molecule	Excited state	Coefficient + MO	λ_{max}	E_{abs}	f_{OSC}	LHE
CAM-B3LYP	PEPH	$S_0 \longrightarrow S_1$	H $\longrightarrow$ L (82.58)	312.2	3.971	0.3617	0.5652
	PPEH	$S_0 \longrightarrow S_1$	H $\longrightarrow$ L (84.29)	314.6	3.941	0.3923	0.5947
ω B97-XD	PEPH	$S_0 \longrightarrow S_1$	H $\longrightarrow$ L (77.21)	300.5	4.126	0.3552	0.5586
	PPEH	$S_0 \longrightarrow S_1$	H $\longrightarrow$ L (74.15)	303.7	4.082	0.3307	0.5330

$E_{abs} \longrightarrow$ excitation energies (in eV), $\lambda_{abs} \longrightarrow$ wavelengths (in nm), $f \longrightarrow$ oscillator strengths, MO $\longrightarrow$ molecular orbital coefficients, H $\longrightarrow$ HOMO, L $\longrightarrow$ LUMO, LHE $\longrightarrow$ light harvesting efficiencies.

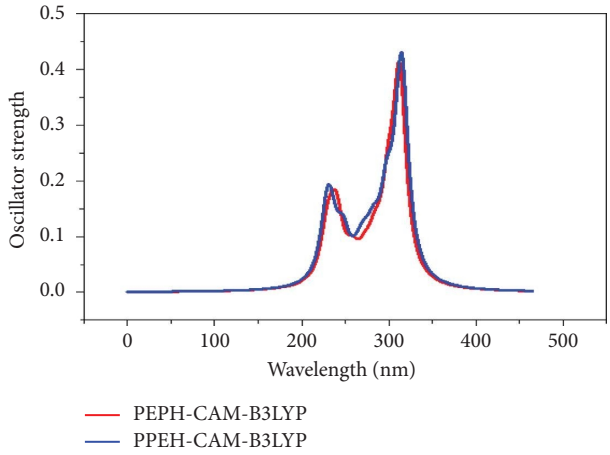

Figure 4: Computed absorption spectra of the investigated compounds obtained at CAM-B3LYP/def2-tzvpp level of theory in the gaseous phase.

expected to produce almost equal amount of photocurrent in OSCs. However, **PPEH** is slightly more effective than **PEPH** at producing a higher photocurrent, owing to its highest oscillator strength. This observation is in accordance with a similar study [45], where the LHE is proportional to the oscillator strength.

The simulated absorption spectra of **PEPH** and **PPEH** in the gaseous phase are shown in Figure 4.

The spectra indicate the most prominent and more intense secondary absorption peak for each molecule.

4. Conclusion

A theoretical study of the geometries, chemical stability, photovoltaic properties, absorption spectra, and nonlinear optic properties of **PEPH** and **PPEH** was carried out using the DFT method and its time-dependent extension (TD-DFT). These molecules have been studied for their potential use in NLO response and as organic solar cell (OSC) components. NLO and OSC property predictions in this work were preceded by structural analysis on the optimized geometries. Due to their higher HOMO and LUMO energy values relative to those of PCBM, along with their higher energy gaps and higher open circuit voltage (V_{oc}), the results suggest that **PEPH** and **PPEH** may function as electron donor materials in OSCs. Also, the ΔE_{L-L} values are greater than 0.3 eV, which predicts the possibility of photo-excited electron transfer from the studied molecules to PCBM, a common requirement in photovoltaic devices. From the results obtained, the static first and second hyperpolarizabilities of **PEPH** (3.07×10^{-30} esu and 4.16×10^{-35} esu, respectively), **PPEH** (3.36×10^{-30} esu and 4.28×10^{-35} *esu*, respectively), and the dynamic NLO response are on average 10 times greater than those of the prototypical NLO molecule, *para*-nitroaniline. The absorption wavelengths of the investigated molecules fall within the ultraviolet (UV) region (100–400 nm) of the electromagnetic (EM) spectrum, indicating that the hydralazine molecules studied may undergo only minimal transparency-nonlinearity trade-off, making them promising lead molecules in the design of NLO and optoelectronic devices.

Data Availability

The data that support the findings of this study are included in the article and in the supplementary data file.

Conflicts of Interest

The authors declare that they have no conflicts of interest regarding the publication of this paper.

Acknowledgments

We gratefully acknowledge the support of the Ministry of Higher Education of Cameroon through its Research Modernization allowance for this project.

Supplementary Materials

The supplementary material contains a figure and tables as a part of this work. Figure S1: linear regression of PEPH and PPEH at B86/Def2-TZVP level of theory. Tables S1 and S2, respectively, contain the DFT/BP86-D3(BJ)/def2-TZVP optimized geometrical Cartesian coordinates of PEPH and PPEH. Table S3 contains computed cationic (E^+), anionic (E^-), and neutral (E^0) energies in eV at B2PLYP-D3(BJ)/def2-tzvpp and M06-2X(D3zero)/def2-tzvpp levels of theory in gas phase. Tables S4–S9 contain the tensor components of the nonlinear properties and susceptibilities. (*Supplementary Materials*)

References

[1] M. K. Wei, C. W. Lin, C. C. Yang, Y. W. Kiang, J. H. Lee, and H. Y. Lin, "Emission characteristics of organic light-emitting diodes and organic thin-films with planar and corrugated structures," *International Journal of Molecular Sciences*, vol. 11, no. 4, pp. 1527–1545, 2010.

[2] R. Jin, X. Zhang, and W. Xiao, "Theoretical studies of photophysical properties of D-π-A-π-D-type diketopyrrolopyrrole-based molecules for organic light-emitting diodes and organic solar cells," *Molecules*, vol. 25, no. 3, p. 667, 2020.

[3] Y. Karzazi and I. Arbouch, "Inorganic photovoltaic cells: operating principles, technologies and efficiencies-Review," *Journal of Materials and Environmental Science*, vol. 5, no. 5, pp. 1505–2525, 2014.

[4] P. Mahalingavelar, "How end-capped acceptors regulate the photovoltaic performance of the organic solar cells: a detailed density functional exploration of their impact on the A–d–π–D–A type small molecular electron donors," *Energy and Fuels*, vol. 36, no. 4, pp. 2095–2107, 2022.

[5] R. Ma, T. Yang, Y. Xiao et al., "Air-processed efficient organic solar cells from aromatic hydrocarbon solvent without solvent additive or post-treatment: insights into solvent effect on morphology," *Energy and Environmental Materials*, vol. 5, no. 3, pp. 977–985, 2021.

[6] A. Rasool, S. Zahid, M. Ans, S. Muhammad, K. Ayub, and J. Iqbal, "Bithieno thiophene-based small molecules for application as donor materials for organic solar cells and hole transport materials for perovskite solar cells," *American Chemical Society Omega*, vol. 7, no. 1, pp. 844–862, 2022.

[7] H. Abdulaziz, A. Gidado, A. Musa, and A. Lawal, "Electronic structure and non-linear optical properties of neutral and ionic pyrene and its derivatives based on density functional theory," *Journal of Materials Science Research and Reviews*, vol. 2, no. 3, pp. 1–13, 2019.

[8] W. C. H. Choy, W. K. Chan, and Y. Yuan, "Recent advances in transition metal complexes and light-management engineering in organic optoelectronic devices," *Advanced Materials*, vol. 26, no. 31, pp. 5368–5399, 2014.

[9] M. Paramasivam, R. K. Chitumalla, S. P. Singh et al., "Tuning the photovoltaic performance of benzocarbazole-based sensitizers for dye-sensitized solar cells: a joint experimental and theoretical study of the influence of π-spacers," *Journal of Physical Chemistry C*, vol. 119, no. 30, pp. 17053–17064, 2015.

[10] J. Song, H. Lee, E. G. Jeong, K. C. Choi, and S. Yoo, "Organic light-emitting diodes: pushing toward the limits and beyond," *Advanced Materials*, vol. 32, no. 35, Article ID e1907539, 2020.

[11] X. Song, N. Gasparini, M. Nahid et al., "A highly crystalline fused-ring n-type small molecule for non-fullerene acceptor based organic solar cells and field-effect transistors," *Advanced Functional Materials*, vol. 28, no. 35, Article ID 1802895, 2018.

[12] M. Ans, M. Paramasivam, K. Ayub et al., "Designing alkoxy-induced based high performance near infrared sensitive small molecule acceptors for organic solar cells," *Journal of Molecular Liquids*, vol. 305, Article ID 112829, 2020.

[13] J. Li, C. Sun, A. Tang et al., "Utilizing an electron-deficient thieno[3,4-: C] pyrrole-4,6-dione (TPD) unit as a π-bridge to improve the photovoltaic performance of A-π-D-π-A type acceptors," *Journal of Materials Chemistry C*, vol. 8, no. 45, pp. 15981–15984, 2020.

[14] M. Raftani, T. Abram, W. Loued et al., "The optoelectronic properties of π-conjugated organic molecules based on terphenyl and pyrrole for BHJ solar cells: DFT/TD-DFT theoretical study," *Current Chemistry Letters*, vol. 10, no. 4, pp. 489–502, 2021.

[15] N. K. Nkungli and J. N. Ghogomu, "Concomitant effects of transition metal chelation and solvent polarity on the first molecular hyperpolarizability of 4-methoxyacetophenone thiosemicarbazone: a DFT study," *Journal of Theoretical Chemistry*, vol. 2016, Article ID 7909576, 19 pages, 2016.

[16] E. Lewars, *Computational Chemistry: Introduction To The Theory and Applications of Molecular And Quantum Mechanics*, Springer, Berlin, Germany, 2011.

[17] B. Ali, M. Khalid, S. Asim et al., "Key electronic, linear and nonlinear optical properties of designed disubstituted quinoline with carbazole compounds," *Molecules*, vol. 26, no. 9, p. 2760, 2021.

[18] M. Khalid, R. Hussain, A. Hussain et al., "Electron donor and acceptor influence on the nonlinear optical response of diacetylene-functionalized organic materials (DFOMs): density functional theory calculations," *Molecules*, vol. 24, no. 11, p. 2096, 2019.

[19] I. Sheikhshoaie and S. Saeednia, "synthesis, characterization and nonlinear optical properties of four novel schiff base compounds," *Arabian Journal for Science and Engineering*, vol. 35, 2010.

[20] D. E. Kiven, N. K. Nkungli, S. N. Tasheh, and J. N. Ghogomu, "*In silico* screening of ethyl 4-[(E)-(2-hydroxy-4-methoxyphenyl)methyleneamino]benzoate and some of its derivatives for their NLO activities using DFT," *Royal Society Open Science*, vol. 10, no. 1, Article ID 220430, 2023.

[21] N. S. Tasheh, N. K. Nkungli, and J. N. Ghogomu, "A DFT and TD-DFT study of ESIPT-mediated NLO switching and UV absorption by 2-(2′-hydroxy-5′-methylphenyl) benzotriazole," *Theoretical Chemistry Accounts*, vol. 138, no. 8, pp. 100–117, 2019.

[22] C. T. Tsapi, S. N. Tasheh, N. K. Nkungli, A. D. T. Fouegue, C. I. L. Alongamo, and J. N. Ghogomu, "Exohedral adsorption of N-(4-Methoxybenzylidene) isonicotinohydrazone molecule onto X 12 N 12 nanocages (where X= B and Al) and the effect on its NLO properties by DFT and TD-DFT," *Journal of Chemistry*, vol. 2023, Article ID 5287422, 15 pages, 2023.

[23] C. Wang, D. Sun, K. Zhuo, H. Zhang, and J. Wang, "Simple and green synthesis of nitrogen-sulfur-and phosphorus-co-doped carbon dots with tunable luminescence properties and sensing application," *Royal Society of Chemistry Advances*, vol. 4, no. 96, pp. 54060–54065, 2014.

[24] A. Irfan and A. Mahmood, "Designing of efficient acceptors for organic solar cells: molecular modelling at DFT level," *Journal of Cluster Science*, vol. 29, no. 2, pp. 359–365, 2018.

[25] M. Paramasivam, R. K. Chitumalla, J. Jang, and J. Youk, "The impact of heteroatom substitution on cross-conjugation and its effect on the photovoltaic performance of DSSCs – a computational investigation of linear vs. cross-conjugated anchoring units," *Physical Chemistry Chemical Physics*, vol. 20, no. 35, pp. 22660–22673, 2018.

[26] A. Asif, N. Maqsood, N. Tamam et al., "DFT study of transition metals doped calix-4-pyrrole with excellent electronic and non-linear optical properties," *Computational and Theoretical Chemistry*, vol. 1214, Article ID 113767, 2022.

[27] A. F. Awantu, G. A. Ayimele, J. J. K. Bankeu et al., "Synthesis, molecular structure, anti-plasmodial, antimicrobial and anti-oxidant screening of (E)-1-(Phthalazin-1-yl)-1-[(Pyridin-2-yl) ethylidene] hydralazine and 1-[2-(1-(pyridine-3-yl) ethylidene) hydrazinyl] phthalazine," *International Journal of Organic Chemistry*, vol. 11, no. 3, pp. 91–105, 2021.

[28] J. N. Yong, F. Majoumo-Mbe, M. Samje, and E. N. Nfor, "Synthesis, molecular structure and anti-onchocercal studies of 1-(phthalazin-1 (2H)-one)[(Pyridin-2-yl) ethylidene] hydrazine," *International Journal of Organic Chemistry*, vol. 6, no. 1, 2016.

[29] E. N. Nfor, A. Husian, F. Majoumo-Mbe, I. N. Njah, O. E. Offiong, and S. A. Bourne, "Synthesis, crystal structure and antifungal activity of a Ni (II) complex of a new hydrazone derived from antihypertensive drug hydralazine hydrochloride," *Polyhedron*, vol. 63, pp. 207–213, 2013.

[30] F. Majoumo-Mbe, E. N. Nfor, E. B. Sengeh, R. N. Njong, and O. E. Offiong, "Synthesis, crystal structure and biological activity of 1-(phthalazin-1 (2H)-one)[(Pyridin-2-yl) ethylidene] hydrazone and its cobalt (III) complex," *Communications in Inorganic Synthesis*, vol. 3, no. 3, 2015.

[31] A. Guillén-López, C. Delesma, C. Amador-Bedolla, M. Robles, and J. Muñiz, "Electronic structure and nonlinear optical properties of organic photovoltaic systems with potential applications on solar cell devices: a DFT approach," *Theoretical Chemistry Accounts*, vol. 137, no. 6, pp. 85–15, 2018.

[32] F. Neese, "The ORCA program system," *WIREs Computational Molecular Science*, vol. 2, no. 1, pp. 73–78, 2012.

[33] M. Frisch, G. Trucks, H. Schlegel, G. Scuseria, M. Robb, and J. Cheeseman, "Gaussian 16, Revision B. 01," 2016, https://gaussian.com/relnotes_b01/.

[34] M. Hanwell, D. Curtis, D. Lonie, T. Vandermeersch, E. Zurek, and G. Hutchison, "Avogadro: an advanced semantic chemical editor, visualization, and analysis platform," *Journal of Cheminformatics*, vol. 4, no. 1, p. 17, 2012.

[35] A. D. Becke, "Density-functional exchange-energy approximation with correct asymptotic behavior," *Physical Review A*, vol. 38, no. 6, pp. 3098–3100, 1988.

[36] J. G. Brandenburg, C. Bannwarth, A. Hansen, and S. Grimme, "B97-3c: a revised low-cost variant of the B97-D density functional method," *The Journal of Chemical Physics*, vol. 148, no. 6, Article ID 064104, 2018.

[37] S. Grimme, J. Brandenburg, C. Bannwarth, and A. Hansen, "Consistent structures and interactions by density functional theory with small atomic orbital basis sets," *The Journal of Chemical Physics*, vol. 143, no. 5, Article ID 054107, 2015.

[38] F. Neese, "An improvement of the resolution of the identity approximation for the formation of the Coulomb matrix," *Journal of Computational Chemistry*, vol. 24, no. 14, pp. 1740–1747, 2003.

[39] Y. Zhang, X. Xu, and W. A. Goddard, "Doubly hybrid density functional for accurate descriptions of nonbond interactions, thermochemistry, and thermochemical kinetics," *Proceedings of the National Academy of Sciences*, vol. 106, no. 13, pp. 4963–4968, 2009.

[40] S. Grimme and F. Neese, "Double-hybrid density functional theory for excited electronic states of molecules," *The Journal of Chemical Physics*, vol. 127, no. 15, Article ID 154116, 2007.

[41] J. P. Perdew, M. Ernzerhof, and K. Burke, "Rationale for mixing exact exchange with density functional approximations," *The Journal of Chemical Physics*, vol. 105, no. 22, pp. 9982–9985, 1996.

[42] F. Weigend and R. Ahlrichs, "Balanced basis sets of split valence, triple zeta valence and quadruple zeta valence quality for H to Rn: design and assessment of accuracy," *Physical Chemistry Chemical Physics*, vol. 7, pp. 3297–3305, 2005.

[43] A. Allouche and A. Olson, "Gabedit—a graphical user interface for computational chemistry softwares," *Journal of Computational Chemistry*, vol. 32, no. 1, pp. 174–182, 2011.

[44] J. A. Luceño-Sánchez, A. M. Díez-Pascual, and R. Peña Capilla, "Materials for photovoltaics: state of art and recent developments," *International Journal of Molecular Sciences*, vol. 20, no. 4, p. 976, 2019.

[45] M. Waqas, N. Hadia, A. M. Shawky et al., "Theoretical framework for achieving high Voc in non-fused non-fullerene terthiophene-based end-capped modified derivatives for potential applications in organic photovoltaics," *Royal Society of Chemistry Advances*, vol. 13, no. 11, pp. 7535–7553, 2023.

[46] R. Meenakshi, "Spectral investigations, inhibition efficiency analysis and a TD-DFT study on tuning the light harvesting efficiency (LHE) of heterocyclic 5-nitro-1, 3-benzodioxole as a photosensitizer for dye sensitized solar cells (DSSCs)," *Royal Society of Chemistry Advances*, vol. 6, no. 68, pp. 63690–63703, 2016.

[47] M. Renjith, "Micro-textures in plagioclase from 1994–1995 eruption, Barren Island Volcano: evidence of dynamic magma plumbing system in the Andaman subduction zone," *Geoscience Frontiers*, vol. 5, no. 1, pp. 113–126, 2014.

[48] A. U. Putra, D. Çakmaz, N. Seferoğlu, A. Barsella, and Z. Seferoğlu, "Styryl-based new organic chromophores bearing free amino and azomethine groups: synthesis, photophysical, NLO, and thermal properties," *Beilstein Journal of Organic Chemistry*, vol. 16, no. 1, pp. 2282–2296, 2020.

[49] I. Anis, M. Aslam, Z. Noreen, N. Afza, A. Hussain, and M. Safder, "A review (part A)-general applications of Schiff base transition metal complexes," *International Journal of Current Pharmaceutical Research*, vol. 5, pp. 21–24, 2013.

[50] C. H. A. Alongamo, N. K. Nkungli, and J. N. Ghogomu, "DFT-based study of the impact of transition metal coordination on the charge transport and nonlinear optical (NLO) properties of 2-{[5-(4-nitrophenyl)-1,3,4-thiadiazol-2-ylimino]methyl}phenol," *Molecular Physics*, vol. 117, no. 18, pp. 2577–2592, 2019.

[51] L. R. Domingo, M. Ríos-Gutiérrez, and P. Pérez, "Applications of the conceptual density functional theory indices to organic chemistry reactivity," *Molecules*, vol. 21, no. 6, p. 748, 2016.

[52] K. M. Ervin, I. Anusiewicz, P. Skurski, J. Simons, and W. C. Lineberger, "The only stable state of O2-is the X 2Πg ground state and it (still!) has an adiabatic electron detachment energy of 0.45 eV," *The Journal of Physical Chemistry A*, vol. 107, no. 41, pp. 8521–8529, 2003.

[53] F. K. Bine, N. S. Tasheh, and J. N. Ghogomu, "A quantum chemical screening of two imidazole-chalcone hybrid ligands and their Pd, Pt and Zn complexes for charge transport and nonlinear optical (NLO) properties: a DFT study," *Computational Chemistry*, vol. 09, no. 4, pp. 215–237, 2021.

[54] B. C. Lin, C. P. Cheng, Z.-Q. You, and C.-P. Hsu, "Charge transport properties of tris (8-hydroxyquinolinato) aluminum (III): why it is an electron transporter," *Journal of the American Chemical Society*, vol. 127, no. 1, pp. 66-67, 2005.

[55] N. A. Wazzan, "A DFT/TDDFT investigation on the efficiency of novel dyes with ortho-fluorophenyl units (A1) and incorporating benzotriazole/benzothiadiazole/phthalimide units (A2) as organic photosensitizers with D–A2–π–A1 configuration for solar cell applications," *Journal of Computational Electronics*, vol. 18, no. 2, pp. 375–395, 2019.

[56] D. Add and R. Shilpi, "Numerical simulation of P3HT based organic light emitting diode," *International Journal of Advanced Applied Physics Research*, vol. 5, no. 1, pp. 7–13, 2018.

[57] G. Santra, R. Calinsky, and J. M. L. Martin, "Benefits of range-separated hybrid and double-hybrid functionals for a large and diverse data set of reaction energies and barrier heights," *The Journal of Physical Chemistry A*, vol. 126, no. 32, pp. 5492–5505, 2022.

[58] I. Muhammad Aamir, A. Naila, S. Wajeehah, A. Deeba, I. Faryal, and A. Raice, "Fundamentals of density functional theory: recent developments, challenges and future horizons,"

in *Density Functional Theory*, G.-M. Daniel, Ed., IntechOpen, London, UK, 2021.

[59] X. Shan, A. Ibrahim, Y. Zhou et al., "Luminescent, second-order NLO and magnetic properties of the hydrogen-bond based network derived from 2, 2′-bipyridine-6, 6′-dicarboxylate," *Inorganic Chemistry Communications*, vol. 22, pp. 149–153, 2012.

[60] J. Zhang, H.-B. Li, S.-L. Sun, Y. Geng, Y. Wu, and Z.-M. Su, "Density functional theory characterization and design of high-performance diarylamine-fluorene dyes with different π spacers for dye-sensitized solar cells," *Journal of Materials Chemistry*, vol. 22, no. 2, pp. 568–576, 2012.